This peer-reviewed published paper appears as: Nikolaidou, V., Latreille, P., Lignos, D.G., and Rogers, C.A. (2018). "Seismic Performance Characterization of Wood-Sheathed and Cold-Formed Steel Framed Floor and Roof Diaphragm Structures", ASCE, *Journal of Structural Engineering*, 144(2), p. 04017215, doi: 10.1061/(ASCE)ST.1943-541X.0001962

SEISMIC PERFORMANCE CHARACTERIZATION OF WOOD-SHEATHED / COLD-FORMED STEEL FRAMED FLOOR AND ROOF DIAPHRAGM STRUCTURES

Violetta Nikolaidou[(1)], Patrick Latreille[(2)], Dimitrios G. Lignos[(3)],Colin A. Rogers[(4)]

Keywords: cold-formed steel; diaphragm; in-plane loading; test program; shear response

Abstract

This paper describes a research program involving wood sheathed / cold-formed steel (CFS) framed diaphragm assemblies. The diaphragm's response to in-plane monotonic and reversed cyclic lateral loading is investigated in an effort to characterize the seismic performance of this assembly. The work presented herein focuses on the response to loading of the isolated diaphragm subsystem and serves as a complementary study to a research project involving the dynamic testing of full-scale two-story CFS framed buildings, known as the CFS – NEES project. Laboratory testing included eight 3.66 x 6.1m diaphragm specimens, i.e. four configurations, comprised of oriented strand board (OSB) sheathing screw connected to CFS C-Channel joists. The response to loading is directly related to screw pattern and size, the use of panel edge blocking, and the type of sheathing. By means of a comparison of design and experimental shear strength and stiffness values the provisions of the AISI S400 Standard were

(1) PhD Candidate, McGill University, Department of Civil Engineering and Applied Mechanics, Montreal, Montreal, 817 Sherbrooke Street West, Montreal QC, Canada, H3A 0C3, violetta.nikolaidou@mail.mcgill.ca,
(2) Master's Student, McGill University, Department of Civil Engineering and Applied Mechanics, Montreal, Canada, patrick.latreille@mail.mcgill.ca,
(3) Associate Professor, Swiss Federal Institute in Lausanne (EPFL), School of Architecture, Civil & Environmental Engineering, Lausanne, Switzerland, dimitrios.lignos@epfl.ch,
(4)Corresponding author
Associate Professor, McGill University, Department of Civil Engineering and Applied Mechanics, Montreal, 817 Sherbrooke Street West, Montreal QC, Canada, H3A 0C3, Tel. 514 398-6449, Fax. 514 398-7361

This peer-reviewed published paper appears as: Nikolaidou, V., Latreille, P., Lignos, D.G., and Rogers, C.A. (2018). "Seismic Performance Characterization of Wood-Sheathed and Cold-Formed Steel Framed Floor and Roof Diaphragm Structures", ASCE, *Journal of Structural Engineering*, 144(2), p. 04017215, doi: 10.1061/(ASCE)ST.1943-541X.0001962

shown to be in need of improvement regarding the number of listed diaphragm configurations. Deflection predications at the design load level were considered to be reasonable.

(1) PhD Candidate, McGill University, Department of Civil Engineering and Applied Mechanics, Montreal, Montreal, 817 Sherbrooke Street West, Montreal QC, Canada, H3A 0C3, violetta.nikolaidou@mail.mcgill.ca,
(2) Master's Student, McGill University, Department of Civil Engineering and Applied Mechanics, Montreal, Canada, patrick.latreille@mail.mcgill.ca,
(3) Associate Professor, Swiss Federal Institute in Lausanne (EPFL), School of Architecture, Civil & Environmental Engineering, Lausanne, Switzerland, dimitrios.lignos@epfl.ch,
(4)Corresponding author
Associate Professor, McGill University, Department of Civil Engineering and Applied Mechanics, Montreal, 817 Sherbrooke Street West, Montreal QC, Canada, H3A 0C3, Tel. 514 398-6449, Fax. 514 398-7361

Introduction

A typical construction practice of cold-formed steel (CFS) structures is the stud wall system with vertical members forming the walls and sheathing installed to provide shear resistance to lateral loads (shear walls). A typical floor and roof system is comprised of discretely or continuously braced CFS joists overlaid with wood sheathing, again to provide shear resistance to lateral loads (diaphragms). The seismic design of CFS framed structures focuses mainly on the lateral response of the shear walls, as the primary component of the lateral force resisting system (LFRS), without explicitly accounting for the diaphragm's contribution to the overall seismic response of the structure. Extensive experimental and numerical work realized for the lateral response of shear walls, e.g. Dolan & Easterling (2000), Serrette et al. (2002), Branston et al. (2006), Pan et al. (2011), Shamim et al. (2013), and Peterman et al. (2016), among others, provides a starting point in the effort to characterize the diaphragm behavior under in-plane loading and its contribution to the seismic response of CFS framed buildings, since little research exists for which the diaphragm response is the focal point of the work (NAHRBC 1999, LGSEA 1998). A shear wall is effectively considered as a vertical cantilevered diaphragm (APA 2007); thus, the structural similarity between shear walls and diaphragms enables preliminary assessments of the diaphragm response through use of the shear wall studies. However, the major role of the diaphragm in distributing the lateral forces to the shear walls and the structural difference of the diaphragm's multiple sheathing panels call for an explicit characterization of its seismic response. The design provisions available for CFS framed diaphragms (AISI S400 2015, AISI S100 2016, NIST 2016, CSA S136 2016) are based largely on experimental work on wood assemblies (Tissell and Elliot, 2004, APA 2007); moreover, the North American standard for the seismic design of cold-formed steel structural systems, AISI S400 (2015), contains no seismic design procedure for CFS framed diaphragms for use in Canada. As such, there exists a need for this shortcoming to be addressed in order to ensure the construction of better, safer and cost-effective CFS structures.

The present design process for diaphragms is solely governed by the selection of suitable connections between the sheathing and the framing, as well as between the diaphragm and the shear walls, in order to ensure adequate shear strength and stiffness. Currently, in the AISI S400 Standard design shear strength values are provided based on analytical work by the Light Gauge Steel Engineers Association (LGSEA 1998) (Table F2.4-1, AISI 2015). These design values are dependent on the field and perimeter screw spacing, but not on the screw size, and are available only for a limited number of plywood sheathed / CFS framed diaphragm configurations based on the methodology included in Tissell and Elliot (2004) for wood framing. Moreover, Serrette's and Chau's (2003) work yielded a deflection equation for simply supported diaphragms, which is included in the AISI S400 Standard (Eq. C-F2.4.3-1, AISI 2015). Shear strength and stiffness values were also made available by the National Association of Home Builders Research Center (NAHBRC 1999), which carried out four monotonic tests on CFS framed / oriented strand board (OSB) sheathed diaphragms, and studied the individual sheathing-to-framing connection response. The launch of the CFS – NEES (i.e., Network for Earthquake Engineering Simulation) project in 2010 was in response to the need for advanced seismic design procedures of CFS structures. This major research project involved the dynamic testing of a full-scale two story CFS framed building (Fig. 1), which was conducted by researchers at Johns Hopkins University (Peterman 2014). Particular emphasis was placed on the characterization of the isolated CFS framed / wood sheathed shear walls (Peterman et al. 2016, Liu et al. 2012), whereas the diaphragms in this structure were not specifically instrumented such that their load – deformation response could be measured; nor based on observations, were they reported to have surpassed the elastic range.

The research presented herein aims to provide insight into the complex nature of the seismic response of the diaphragm subsystem. Eight OSB sheathed / CFS framed roof and floor diaphragms were tested, using either monotonic or reversed cyclic loading. The objective was to characterize the diaphragm response to in-plane loading and to obtain information for an isolated diaphragm's seismic performance to supplement the data acquired in the CFS – NEES project. To this end, the diaphragm configurations were based on the floor and roof configurations used in the CFS - NEES Building (Fig. 1). The tests were conducted in the Jamieson Structures Laboratory at McGill University following a cantilever test method, detailed according to the provisions of the AISI S907 Standard (2013) for diaphragm testing, with the overall specimen dimensions being 3.66 m x 6.1 m (Nikolaidou et al. 2015). This paper concludes with a comparison between the measured test values and the calculated shear strength and deflection values following the AISI S400 North American Standard (2015) for the seismic design of cold-formed steel structural systems.

CFS Framed Diaphragm Test Program

The research program required the design and construction of a setup to accommodate the diaphragm tests (Figures 2 and 3). It consisted of a pin-connected self-reacting braced frame with wide-flange (W-shape) sections as the main beams and double angle sections as the bracing. The design aimed for the frame to remain elastic during the test and to have adequate stiffness to exhibit the minimum possible deformation, i.e. span-length / 1125. A 450 kN (tension) / 650 kN (compression) actuator, hinged at both ends, was attached to a force distribution beam, which was in turn bolted to one side of each diaphragm specimen. The support of the distribution beam comprised a roller system at three locations, which allowed it to move freely. Thus, in combination with the hinged actuator, the diaphragm specimen could also move (lengthen and shorten) perpendicular to the direction of the applied loading. The specimen was fixed along the other side to the frame. Selected photographs of the test specimen and setup are provided in Figure 4.

The roof and floor diaphragms of the CFS - NEES Building had the following characteristics: steel thickness 1.37 mm vs. 2.46 mm, #8 vs. #10 sheathing screws and OSB panel thickness 11.1mm vs. 18.2mm with tongue and groove (T&G) edges, respectively (Table 1). Neither of the diaphragms included edge blocking, i.e. CFS framing under all of the OSB panel edges. Following the CFS - NEES Building design, the first two diaphragm test configurations incorporated these construction details (Fig. 5). Subsequently, a construction parameter was altered in each configuration: i) full panel edge blocking was added to the roof configuration (full height blocking with joist sections as shown in Fig. 6), where the full perimeter of each OSB panel was fastened to the underlying steel framing, and ii) a larger sheathing screw size (#12) was used in the floor configuration. The objective was to investigate the effect of these two parameters on the shear strength and stiffness of the diaphragm. Monotonic and reversed cyclic loading was employed for each of the four configurations. The bare CFS framing without the sheathing was also tested under monotonic loading in order for its contribution to be accounted for separately. In total, the four diaphragm configurations, each tested with two loading protocols, and the two bare frame tests resulted in a laboratory program comprising 10 tests.

The material used for the fabrication of the joists and tracks was ASTM A653 (2015) Grade 50 (i.e. nominal yield stress F_y = 345MPa) steel. Moreover, Figure 5 demonstrates the following two features of the diaphragm specimens: a double CFS joist section as a chord element to represent the presence of a wall in actual conditions (increased stiffness) and a 152.4mm sheathing extension at the fixed connection location, as per the CFS - NEES building design for ledger framing. This led to an out-to-out width of the CFS frame of 3505mm. Figure 7 illustrates the connections used to connect the CFS framing, while Table 2 includes the nomenclature followed for the specimens.

The CUREE displacement controlled loading protocol for ordinary ground motions (Krawinkler et al. 2000), which represents an earthquake excitation with a probability of exceedance of 10 % in 50 years, was selected for the reversed cyclic tests (i.e. Fig. 8 depicts the loading protocol for the roof blocked specimen 8). A specific loading protocol for CFS framed diaphragms was not available; since the CUREE protocol had been extensively used for the testing of the CFS framed shear walls relied on in the development of the AISI S400 Standard, it was decided to also use it for this study. The effect of cumulative damage is taken into account with the repetition of multiple small deformation amplitude loading cycles followed by larger deformation amplitudes. The protocol is based on a post peak reference displacement obtained from the monotonic test at 80% of the ultimate load. A displacement rate of 2.5mm/min for the roof and 5mm/min for the floor configuration was applied during the monotonic loading, while the cyclic loading followed a displacement rate that started with 15mm/min and increased to 60mm/min after 60mm of displacement for both the roof and floor configurations.

Regarding the instrumentation employed, lateral displacement and shear deformation as well as local in-plane displacement were captured using four string potentiometers (254 mm & 508 mm total stroke) and twelve linear variable differential transformers (LVDTs ±15 mm stroke), as shown in Figure 9. The diaphragm response was also captured by the internal LVDT and load cell of the actuator. Vishay Model 5100B scanners and the Vishay System 5000 StrainSmart software were used to record the measured data.

Material Properties

Tensile coupon tests and moisture content measurements were conducted for the steel and wood material used in the experiments, respectively. The tensile coupon tests were based on the ASTM A370 Standard (2016) while the secondary oven-drying method of the ASTM D4442 Standard Method B (2015) was employed for the moisture content measurements. Coupons (50mm gauge length) were extracted from the CFS sections considering the different steel thicknesses (roof rim joist, roof joist, floor rim joist, floor joist). An average value was obtained for each tensile material property from three coupons for each case. Strain gauges and an extensometer were utilized to measure Young's modulus and elongation values. The nominal yield stress and tensile strength of the ASTM A653 Grade 50 steel was 345MPa and 450MPa, respectively. Table 3 summarises the results from the tensile coupon tests. Sharp yielding behavior was observed for all the coupon specimens with increased yield stress values expected due to the fabrication process of cold-formed steel (cold work of forming). For the moisture content measurements, samples from the OSB panels were placed for 24 hours in a constant oven temperature of 103^{o}C in order for the oven - dry mass to be obtained (ASTM D4442 2015, Method B). Three round specimens per panel (76.2mm in diameter) were extracted from selected panels immediately after testing and their weight was measured. Low moisture content in the range of 4% to 5% was obtained, as expected due to the fabrication process of the OSB panels.

Diaphragm Test Results

The hysteretic and monotonic shear force vs. deformation response was obtained for all diaphragm configurations, starting with the monotonic testing of the bare CFS frame without the sheathing. A maximum displacement of 45mm was targeted for the bare CFS framing loading to ensure that the specimen would remain in the elastic range. These tests revealed that the shear strength and stiffness contribution of the bare CFS frame is negligible, as indicated in Figure 10. A photograph showing the typical overall shear deformations of a wood sheathed / CFS framed diaphragm is provided in Figure 11; in this case Test 10-F #12-C. Subsequently, the monotonic results for specimens 3-RU-M, 4-RU-C, 5-F #10-M and 6-F #10-C are presented in Figures 12a and 15a in the form of a comparison between shear response vs. rotation curves. Figure 12b includes the blocked vs. unblocked roof diaphragm configuration reversed cyclic results (7-RB-M, 8-RB-C vs. 3-RU-M,4-RUC), while Figure 15b contains a comparison of the floor with #12 sheathing screws vs. the floor with #10 screws (9-F#12-M, 10-F#12-C vs. 5-F#10-M,6-F#10-C), respectively. Referring to Figures 12b and 15b, the equivalent monotonic curve is superimposed for specimens 7 and 9, respectively. It is shown that there is no difference between the diaphragm's monotonic and the cyclic response up to the ultimate shear strength level; as expected the post peak cyclic curve deteriorates more quickly due to the cumulative damage of the repeated displacement cycles. This cumulative damage also results in the lower resistance attained for the negative displacement cycles. The damage to the specimens, a result of the in-plane shear loading, is illustrated in Figures 13, 14 and 16. Table 4 summarises the corresponding data for all the tests. Details of the behavior exhibited by the specimens are provided in the following paragraphs. It should also be mentioned that the displacement shown in the graphs was obtained from the string potentiometer (N-S S_{SP}, Fig. 9) recording the displacement of the specimen in the north-south direction. The rotation was obtained by dividing this displacement with the end members' length, 3505mm.

Roof configuration test results

The failure modes observed during the testing of specimens 3-RU-M and 4-RU-C were the screws tearing out or pulling through the wood after wood bearing had occurred (Fig.13a). Tilting of the screws was present as a desirable ductile deformation mode. Damage concentrated mostly in the middle row of the panels, where fewer screws were used (unblocked diaphragm, 304mm screw spacing). Toward the end of the test lift-off of the OSB panels was triggered in the intermediate panel locations along their edges where the sheathing was no longer attached to the framing, as illustrated in Fig. 13b.

Adding panel edge blocking to the roof diaphragm configuration (specimens 7-RB-M, 8-RB-C) had a profound effect on the diaphragm response (Fig. 12). This configuration yielded a 130% increase in maximum shear strength and a 70% increase in shear stiffness compared to the unblocked case (Table 4). The blocked roof diaphragm configuration exhibited the highest shear strength and stiffness overall in this experimental program even though the OSB was thinner and the sheathing screws smaller than for the floor configuration. The benefit of attaching the full perimeter of each OSB panel to the underlying CFS framing was demonstrated. In this case similar failure modes to the unblocked case (Figure 14a) were observed (tear-out and pull-through) accompanied by sheared fasteners mostly in areas where the fasteners penetrated two layers of steel (joist-to-rim joist connection locations). After the peak load was reached, the damage concentrated in the sheathing screw connections along the fixed edge of the test setup (Fig. 14b). Due to the 152mm extension of the OSB in that location, as explained earlier, a shorter width panel was connected to the steel framing; thus, fewer screws were used, which potentially led to the concentration of sheathing connection failures. Ultimately, the sheathing connections in these edge panels failed, resulting in a transfer of force through the underlying steel framing by means of bending action (cantilever moment frame action of the steel framing in that location since there was no more diaphragm action, Fig. 14b). This bending action of the steel framing is the cause of the constant level of the shear force after approximately 25 mrad rotation indicated in the response curves in Fig. 12a and b.

Floor configuration test results

During the testing of specimens 5-F#10-M and 6-F#10-C a steeper decline of the shear strength vs. deformation curve (Fig. 15) was observed compared to specimen 3-RU-M and 4-RU-C, attributed to the fact that the #10 sheathing screws were primarily failing in shear or remaining vertical while the wood sheathing was tearing out. This sheathing screw behavior suggested that the #10 screws (5-F#10-M, 6-F#10-C, Fig. 16a) used thus far for this type of floor configuration were not appropriate based on the sheathing and steel thickness if a more ductile failure mode were desired. Moreover, at approximately 35mrad (Fig. 15a and b) most of the screws in the interface of the panel rows and field had failed leading to the CFS framing underneath taking most of the load. The load increasing and then stabilizing during these final excursions showed that contact/bearing action along the edges of the intermediate panels provided additional resistance, taking also into account the T&G characteristic of the OSB panels, which prevented lift-off of panels even though the panel edges were not blocked. A finite element model of the floor diaphragm specimen (5-F#10-M and 6-F#10-C) described in Chatterjee (2016) revealed that the level of static friction force developed during testing in the intermediate panel locations was 0.003kN/mm, which provides a minimum level of contact force being present of 0.0075kN/mm, assuming an average coefficient of friction for a wood-to-wood surface of 0.4

(Giancoli 2009). Further, the T&G panels facilitated the construction process (walking on top of the diaphragm) and, thus, would be a useful improvement for the design of the roof diaphragm. The floor configuration, comprised of greater thickness steel and sheathing, was expected to return higher shear strength and stiffness values compared to the roof configuration, as presented in Table 4. Figure 16 illustrates the failure mode and panel edge contact effect for the 5-F#10-M and 6-F#10-C specimens described herein.

The larger screw size (#12 vs. #10) for the floor configuration (9-F#12-M &10-F#12-C) resulted in an overall increase of 50% in shear strength (Table 4). Screw tilting was present before shearing or pulling out of the steel due to shear and tensile forces developing between the CFS framing and OSB panels. Several joist flanges were distorted due to these applied uplift forces of the panels. Although there was an evident increase in strength due to the #12 sheathing screws, based on Figure 15, the overall force vs. deformation response was similar in shape for the two diaphragms, but the observed response of the sheathing connection seemed to be more ductile since shear fracture of the screws did not take place in the 9-F#12-M and C specimens.

Diaphragm Design Predictions

The AISI S400 Standard (2015) provides a diaphragm deflection equation for simply supported span-lengths (Eq. C-F2.4.3-1) and a shear wall deflection equation (E1.4.1.4-1). Given the cantilever approach utilised in the test, it was deemed appropriate for the shear wall deflection equation to be used in order to acquire design deflection values for the diaphragm configurations. Ultimately, it was revealed that both equations provide similar results, given the appropriate assumptions, and are presented in this paper (Eq. 1 for cantilever shear wall and Eq. 2 for simply supported diaphragm in this paper, respectively; see notation list). Design deflection values were acquired for the design shear strength level following both the Canadian and US code; a resistance factor ϕ of 0.6 for Load and Resistance Factor Design (60% of strength) and a safety factor Ω of 2.5 for Allowable Strength Design (40% of strength) was considered, respectively (AISI S400 Standard 2105). Equations 1 and 2 translate into the following components of the diaphragm/shear wall response (AISI S400 (2015)): i) linear elastic bending (1st term), ii) linear elastic shear deformation (2nd term), iii) nonlinear empirical component (3rd term), and iv) overturning anchorage/ chord splice deformation.

$$\delta = \frac{2vh^3}{3E_sA_cb} + \frac{\omega_1\omega_2vh}{\rho Gt_{sheathing}} + \omega_1^{\frac{5}{4}}\omega_2\omega_3\omega_4\left(\frac{v}{\beta}\right)^2 + \frac{h}{b}\delta_v \quad (1)$$

$$\delta = \frac{0.052vL^3}{E_sA_cb} + \frac{\omega_1\omega_2vL}{\rho Gt_{sheathing}} + \omega_1^{\frac{5}{4}}\omega_2(a)\left(\frac{v}{2\beta}\right)^2 + \frac{\sum_{j=1}^{n}\Delta_{ci}X_i}{2b} \quad (2)$$

Equation 1: The shear wall deflection equation refers to the deflection of a blocked CFS framed/wood sheathed shear wall. The δ_v variable referring to the anchorage deformation was obtained using the data of the string potentiometer in the E-W direction (E-W S_{SP}, Fig. 9), which provided the chord member deformation, since no anchorage details were included in the diaphragm specimens.

Equation 2: The diaphragm deflection equation refers to the deflection of a blocked CFS framed/wood sheathed simply supported diaphragm. As such, the total shear load applied was assumed to be 2V and the total length of the diaphragm L = 2*3505 = 7010mm, since the deflection obtained for a cantilever under point load P is equal to the one obtained by a simply supported beam at mid-span with double the cantilever length and under a load 2P. The Δ_{ci} variable referring to the chord splice deformation was obtained using the data of the string potentiometer in the E-W direction (E-W S_{SP}, Fig. 8), as for Eq. 1. The splice was assumed to be in the middle of the chord; thus, X_i = 3505mm. It should be noted that the shear modulus values employed in the calculations (i.e. G = 1317 N/mm^2 for the roof specimens) were obtained from TECO's document entitled Design Capacities for Oriented Strand Board (TECO 2008). Further, an amplification factor of 2.5 is suggested for the diaphragm deflection equation (Eq. C-F2.4.3-1 AISI S400 (2015)) when the diaphragm is unblocked. Such factor does not exist for the shear wall deflection (E1.4.1.4-1 AISI S400 (2015)) equation since a shear wall is always blocked. However, since both equations yield similar results and refer to a diaphragm in this paper the 2.5 factor is applied to both.

Table 5 provides the results for Eq. 1 and 2 compared to the observed values from testing corresponding to the design level of 40% and 60% of the shear strength. It is shown that Eq. 1 and 2 provide similar results and that in almost all the cases the error between calculated and observed data is close to 20% or lower. Further, looking at the error percentages of Table 5 and the force vs. deformation curves of Figures 12 and 15, it can be observed that the error is reduced when the level of force considered for calculation corresponds to the near linear part of the curve, which indicates that Eq. 1 and 2 can confidently be used to calculate deflection at the design shear strength level but may not produce as accurate results for the peak shear strength level. Included in Table 5 is the relative error of calculated displacements with respect to measurements. It should be noted that a different process was followed compared to the one presented in Nikolaidou et al. (2017), in which the focus was to compare the deflection design values at the ultimate shear strength level with an equivalent elastic displacement, $\delta_{elastic}$, provided by the experimental data at ultimate assuming elastic response of the diaphragm. This effort led to this updated process were only the design level shear strength was considered and appropriate assumptions were made for both deflection equations leading to more reasonable results.

Table 6 lists the nominal shear resistance values, V_{AISI}, as obtained from Table F2.4-1 of the AISI S400 Standard (2015) to be used in design and the measured shear resistance values, V_{TEST}, provided from the tests for each diaphragm configuration presented herein. Table F2.4-1 refers only to plywood sheathing and does not account for the effect of the sheathing screw size; thus, meaningful design predictions cannot be made for the specific tested diaphragm specimens. Nonetheless, these are the only design shear strength values available at present in the AISI S400 Standard (2015) for the tests included in this paper.

Conclusions

A total of ten CFS framed / OSB sheathed diaphragm tests were completed in the experimental program described in this paper. The research focused on four main diaphragm configurations, for which various parameters were altered, such as the steel section and the OSB thickness, the screw size and the use of panel edge blocking. The objective was to characterize the in-plane force vs. deformation response of the CFS framed / wood sheathed diaphragm under monotonic and reversed cyclic loading. The main findings are summarised as follows:

- Panel edge blocking substantially increases the diaphragm shear strength and stiffness, with values of 130% and 70% obtained, respectively, for the roof configuration.
- Changing the sheathing screw size from #10 to #12 does not have a measurable effect on the shape of the overall diaphragm load vs. displacement response despite the fact that it leads to a somewhat more ductile sheathing–to–framing screw connection behavior. It does cause, however, a considerable increase in the diaphragm shear strength (50%).

- As tested, the CFS floor and roof framing without the sheathing does not contribute to the shear strength and stiffness of the diaphragm.
- T&G sheathing panels improve both the construction process and the performance of the diaphragm. As such, their further implementation also for roof diaphragms should be considered.
- In an effort to obtain design shear and deflection values the AISI S400 Standard (2015) was employed. The design deflection values calculated using the shear wall and diaphragm deflection equations (Eq. 1 and 2 in this paper) of the AISI S400 Standard (2015) were in close proximity with the experimental values for the design level shear strength of the specimens. However, regarding design shear strength values, the AISI S400 Standard (2015) at present does not include values for the case of OSB panels, and the size of the screws is not considered as an influential parameter in the design shear strength calculations. As such, relevant design shear strength values could not be obtained.

Additional experimental and numerical work is required in order for complete information about the CFS framed diaphragm response to be available to professional engineers. Studies should focus on varying parameters, such as screw spacing, load direction, panel blocking type and panel type, as well as implementing non-structural components, such as gypsum panels.

Acknowledgements

The authors would like to thank the American Iron and Steel Institute (AISI) for financially supporting this research project. Additional support was obtained from the Canadian Sheet Steel Building Institute (CSSBI) and the Natural Sciences and Engineering Research Council of Canada (NSERC). A special thank you is also extended to Bailey Metal Products Ltd., Simpson Strong-Tie Co. Inc., Ontario Tools and Fasteners Ltd, ArcelorMittal and Constructions Proco Inc. for the materials and tools that were provided.

Notation

The following symbols are used in this paper:

A_c = Gross cross-sectional area of chord member (mm^2)

b = Width of the shear wall/diaphragm (parallel to loading) (mm)

E_s = Modulus of elasticity of steel 203,000 MPa

G = Shear modulus of sheathing material (MPa)

h = Wall height (mm)

K = Rigidity of diaphragm specimen calculated at 40% shear strength (kN/mm)

L = Diaphragm length perpendicular to direction of load (mm)

n = Number of chord splices in diaphragm (considering both diaphragm chords)

s = Maximum fastener spacing at panel edges (mm)

S_u = Shear strength of diaphragm specimen (kN/m)

$t_{sheathing}$ = Nominal panel thickness (mm)

t_{stud} = Nominal framing thickness (mm)

V = Total in-plane load applied to the diaphragm (N)

v = Shear demand (V/b), (N/mm)

X_i = Distance between the "i^{th}" chord-splice and the nearest support (mm)

α = 1 for a uniformly fastened diaphragm

β = 2.35 for plywood and 1.91 for OSB for SI units ($N/mm^{1.5}$)

Δ_{ci} = Deformation value associated with "i^{th}" chord splice (mm)

$\Delta_{net,o4u}$ = Displacement value of diaphragm specimen at 40% shear strength (mm)

$\Delta_{net,u}$ = Displacement value of diaphragm specimen at ultimate shear strength (mm)

δ = Calculated in-plane deflection (mm)

δ_v = Vertical deformation of anchorage / attachment details (mm)

$\theta_{net,u}$ = Rotation of diaphragm specimen at ultimate strength, $\Delta_{net,u}$ / 3505mm (rad x 10^{-3})

ρ = 1.85 for plywood and 1.05 for OSB, term for different sheathing material type

ω_1 = s/152.4 (for s in mm)

ω_2 = 0.838/t_{stud} (for t_{stud} in mm)

ω_3 = $\sqrt{(h/b)/2}$

ω_4 = 1 for wood with structural panels

References

AISI (American Iron and Steel Institute). (2015). "North American standard for seismic design of cold-formed steel structural systems." *AISI S400*, Washington, DC.

AISI (American Iron and Steel Institute). (2016). "North American specification for the design of cold-formed steel structural members." *AISI S100*, Washington, DC.

AISI (American Iron and Steel Institute). (2013). "Test standard for cantilever test method for cold-formed steel diaphragms". *AISI S907*, Washington, DC.

APA (The Engineered Wood Association). (2007). "*Diaphragms and shear walls*." Design/Construction Guide Form No. L350A.

ASTM (American Society for Testing and Materials). (2016). "Standard test methods and definitions for mechanical testing of steel products." *ASTM A370*, West Conshohocken, PA.

ASTM (American Society for Testing and Materials). (2015). "Standard specification for steel sheet, zinc-coated (galvanized) or zinc-iron alloy-coated (galvannealed) by the hot-dip process." *ASTM A653*, West Conshohocken, PA.

ASTM (American Society for Testing and Materials). (2015). "Standard test methods for direct moisture content measurement of wood and wood base materials." *ASTM D4442*, West Conshohocken, PA.

Branston, A. E., Boudreault, F. A., Chen, C. Y., & Rogers, C. A. (2006). "Light-gauge steel-frame wood structural panel shear wall design method." *Canadian Journal of Civil Engineering*, *33*(7), 872-889.

Chatterjee A. (2016). "Structural system reliability with application to light steel-framed buildings." *PhD Thesis*, Virginia Polytechnic Institute and State University, Blacksburg, Virginia.

CSA (Canadian Standards Association). (2016). "North American specification for the design of cold-formed steel structural members." *CSA S136*, Rexdale, Canada.

CSI (Computers and Structures, Inc). (2009). "Linear and non-linear static and dynamic analysis and design of three-dimensional structures basic analysis reference manual." *SAP2000 V.14*, Berkeley, CA.

Dolan, J.D., and Easterling, W.S. (2000). "Monotonic and cyclic tests of light-frame shear walls with various aspect ratios and tie-down restraints". Report No. TE-2000-001, Virginia Polytechnic Institute and State University, Blacksburg, VA.

Giancoli, D. (2009). "*Physics for Scientists and Engineers with Modern Physics*," Pearson Education, Inc, 4th Edition.

Krawinkler, H., Parisi, F., Ibarra, L., Ayoub, A., Medina, R. (2000). "Development of a testing protocol for wood frame structures." *Report W-02 covering Task 1.3.2*, CUREE/Caltech Woodframe Project. Consortium of Universities for Research in Earthquake Engineering (CUREE), Richmond, CA.

LGSEA (Light Gauge Steel Engineers Association). (1998). "Lateral load resisting elements: Diaphragm design values." *Tech Note 558b-1*, Washington, DC.

Liu, P., Peterman, K.D., Yu, C., Schafer, B.W. (2012). "Cold-formed steel shear walls in ledger-framed buildings." *Annual Stability Conference, Structural Stability Research Council*, Grapevine, TX.

NAHB Research center (1999). "Innovative residential floor construction: Horizontal diaphragm values for cold-formed steel framing." *U.S. Department of Housing and Urban Development,* Upper Marlboro, MD.

Nikolaidou, V., Latreille, P., Rogers, C.A. and Lignos, D.G. (2017). "Characterization of cold-formed steel framed/wood-sheathed floor and roof diaphragm structures*", Paper number 452, 16th World Conference on Earthquake Engineering*, Santiago, Chile.

Nikolaidou, V., Latreille, P., Rogers, C.A. and Lignos, D.G. (2015). "Characterization of CFS framed diaphragm behavior." *Report CM – 432*, American Iron and Steel Institute, Washington, DC.

NIST, Madsen R.L., Castle T.A. and Schafer B.W. (2016). "Seismic design of cold-formed steel lateral load resisting systems: A guide for practicing engineers." GCR 16-917-38, NEHRP Seismic Design Technical Brief No. 12, produced by the Applied Technology Council and the Consortium of Universities for Research in Earthquake Engineering for the National Institute of Standards and Technology, Gaithersburg, MD

Pan, C. L. and Shan, M. Y. (2011). "Monotonic shear tests of cold-formed steel wall frames with sheathing." *Thin-Walled Structures*, *49*(2), 363-370.

Peterman, K. D., Stehman, M. J., Madsen, R. L., Buonopane, S. G., Nakata, N., and Schafer, B. W. (2016). "Experimental seismic response of a full-scale cold-formed steel-framed building. I: System-level response." *ASCE Journal of Structural Engineering*, 142(12): 04016127.

Peterman, K. D., Stehman, M. J., Madsen, R. L., Buonopane, S. G., Nakata, N., and Schafer, B. W. (2016). "Experimental seismic response of a full-scale cold-formed steel-framed building. II: Subsystem-level response." *ASCE Journal of Structural Engineering*, 142(12): 04016128.

Peterman, K.D. (2014). "Behavior of full-scale cold-formed steel buildings under seismic excitations." *PhD Thesis*, Johns Hopkins University, Baltimore, MD.

Serrette, R.L, Morgan, K.A., and Sorhouet, M.A. (2002). "Performance of cold-formed steel-framed shear walls: Alternative configurations". *Report No. LGSRG-06-02*, Santa Clara University, Department of Civil Engineering, Santa Clara, CA.

Serrette, R.L., and Chau, K. (2003). "Estimating the response of cold-formed steel-frame shear walls." Santa Clara University, Department of Civil Engineering. Santa Clara. CA

Shamim, I., DaBreo, J., & Rogers, C. A. (2013). "Dynamic testing of single-and double-story steel-sheathed cold-formed steel-framed shear walls." *Journal of Structural Engineering*, *139*(5), 807-817.

TECO (2008). "TECHTIP. Design capacities for oriented strand board". Retrieved June 27th, 2017, from www.pfsteco.com/techtips/pdf/tt_osbdesigncapacities.

Tissell, J. R. and Elliot, J. R. (2004). "Plywood diaphragms." *Research Report 138*, American Plywood Association (APA), Tacoma, WA.

Table 1. Basic floor and roof diaphragm configurations

Roof Diaphragm Component	Section (mm)	Length (mm)
Joists	305S51-137M	3505
Rim Joists	305T51-173M	6480
Web Stiffeners	L 38x38x1.37	250
Joist bracing	305S41-137M	560
Joist bracing connectors	L 38x102x1.37	250
Straps	38x1.37	6300
#8 sheathing self-drilling (152/305mm spacing)	-	50
#10 steel-to-steel flat head self-drilling	-	20
#10 steel-to-steel Hex Head Cap self-drilling	-	25
OSB panels (24/16 rated)	2400x1200x 11	-
Floor Diaphragm Component	**Section (mm)**	**Length (mm)**
Joists	350S64-246M	3505
Rim Joists	350T64-246M	6480
Web Stiffeners	L 38x38x1.37	280
Joist bracing	305S51-137M	550
Joist bracing connectors	L 38x102x1.37	250
Straps	38x1.37	6300
#10 sheathing self-drilling (152/305mm spacing)	-	44
#10 steel-to-steel flat head self-drilling	-	20
#10 steel-to-steel Hex Head Cap self-drilling	-	25
OSB panels (48/24 rated T&G)	2400x1200x 18	-

Table 2. Specimen nomenclature

Specimen	Description
1-RF-M	Roof Bare Steel Frame Monotonic
2-FF-M	Floor Bare Steel Frame Monotonic
3-RU-M	Roof Unblocked Monotonic
4-RU-C	Roof Unblocked Cyclic
5-F#10-M	Floor #10 Screws Monotonic
6-F#10-C	Floor #10 Screws Cyclic
7-RB-M	Roof Blocked Monotonic
8-RB-C	Roof Blocked Cyclic
9-F#12-M	Floor #12 Screws Monotonic
10-F#12-C	Floor #12 Screws Cyclic

Table 3. Tensile properties of steel

Specimens	E (MPa)	F_y (MPa)	ε_y (mm/mm)	F_u (MPa)	ε_u (mm/mm)	F_u/F_y	Elongation (%)	No.
RJ - Roof	188595	387	0.0040	466	0.1717	1.20	27.5	3
RJ - Floor	224149	398	0.0028	474	0.1822	1.19	31.8	3
J - Roof	189049	391	0.0037	471	0.1959	1.20	28.7	3
J - Floor	210854	394	0.0036	462	0.1695	1.17	29.3	1
J - Roof B	200568	385	0.0015	466	0.0673	1.21	14.8	3
J – Floor #12	202097	410	0.0018	477	0.0858	1.16	14.6	3

Note: RJ = Rim Joist, J = Joist, B = Blocked, #12 = size #12 sheathing screws

Table 4. General results from the monotonic (M) and reversed cyclic (C) tests

Specimens	S_u (kN/m)	$\Delta_{net,o.4u}$ (mm)	$\Delta_{net,u}$ (mm)	$\theta_{net,u}$ (rad x 10^{-3})	Rigidity, K (kN/mm)
3-RU-M	5.6	9	41.5	11.8	1.53
5-F#10-M	7.9	6.1	30	8.6	3.15
7-RB-M	13	12	62.1	17.7	2.64
9-F#12-M	11.8	9.4	60.7	17.3	3.07
4-RU-C	5.5/-5.1	7.5/-6.9	41.2/-30.6	11.8/-8.7	1.79/1.81
6-F#10-C	7.6/-7.1	5.8/-6.7	30.8/-23.4	8.8/-6.7	3.18/2.57
8-RB-C	13/-10.7	13.1/-11.1	65.5/-45	18.7/-12.8	2.48/2.34
10-F#12-C	11.8/-11	8.8/-9.1	57.1/-40.7	16.3/-11.6	3.29/2.93

Table 5. Design deflection values using Eq. 1 and 2

Deflection At 40% Strength	**3-RU-M & 4-RU-C**	**5-F#10-M & 6-F#10-C**	**7-RB-M & 8-RB-C**	**9-F#12-M & 10-F#12-C**
$\delta_{Observed}$ (mm)	8.18	5.61	10.6	7.82
$\delta_{Calculated}$(mm), Eq. 1	8.46	4.68	8.67	9.59
% Error	3.4	16.6	18.2	22.7
$\delta_{Calculated}$(mm), Eq. 2	8.59	4.52	8.06	8.83
% Error	5.1	19.4	23.9	12.9
Deflection At 60% Strength	**3-RU-M & 4-RU-C**	**5-F#10-M & 6-F#10-C**	**7-RB-M & 8-RB-C**	**9-F#12-M & 10-F#12-C**
$\delta_{Observed}$ (mm)	13.52	9.61	17.4	15.32
$\delta_{Calculated}$(mm), Eq. 1	13.72	10.54	14.4	17.32
% Error	1.5	9.7	17.2	13
$\delta_{Calculated}$(mm), Eq. 2	13.48	9.81	12.53	15.03
% Error	0.3	2.1	28	1.9

Table 6. Nominal shear resistance values using Table F2.4-1 of AISI S400 (2015)

Shear Resistance	3-RU-M & 4-RU-C	5-F#10-M & 6-F#10-C	7-RB-M & 8-RB-C	9-F#12-M & 10-F#12-C
V_{AISI} (kN/m)	7.37	8.10	11.10	8.10
V_{TEST} (kN/m)	5.6	7.9	13	11.8

List of Figures

a) b)

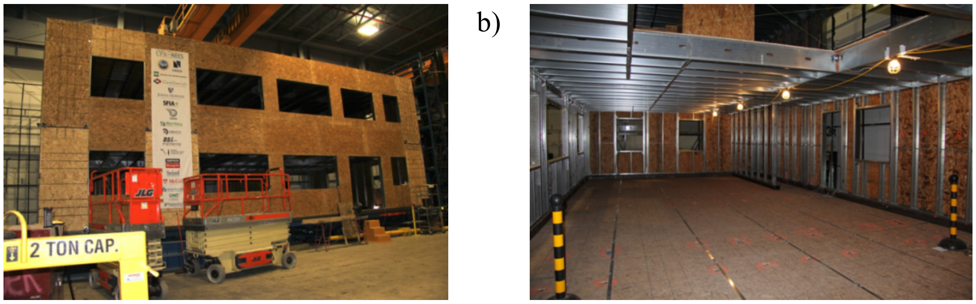

Fig. 1. CFS – NEES Building; a) elevation, and b) ground floor (courtesy of Dr. Kara Peterman, University of Massachusetts Amherst)

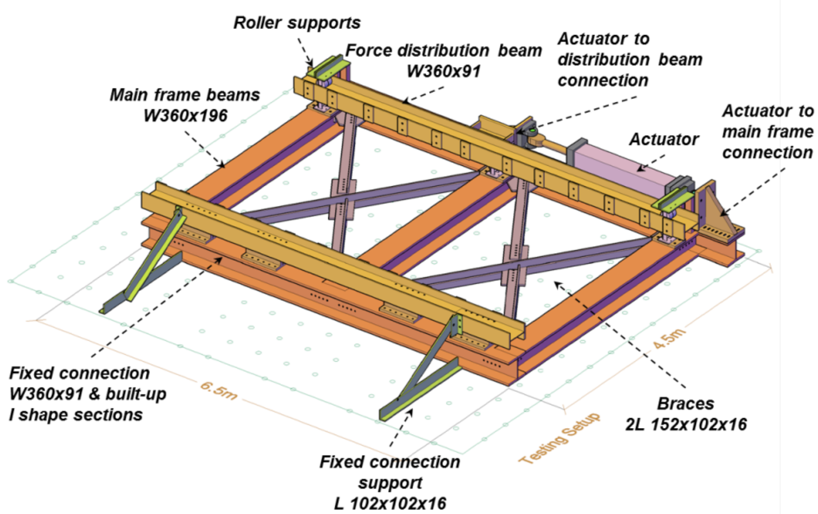

Fig. 2. CFS diaphragm test setup

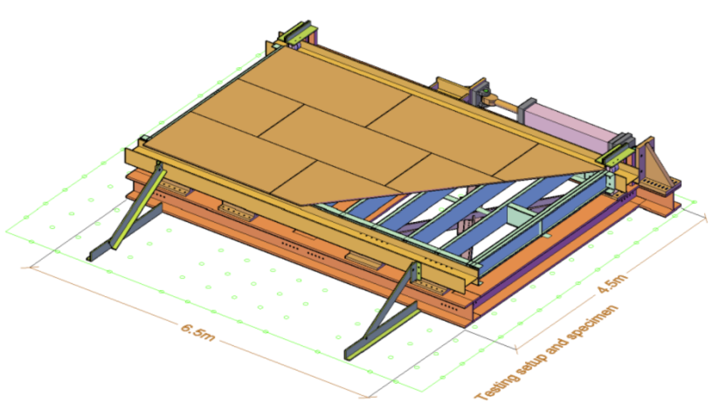

Fig. 3. CFS diaphragm test specimen and setup

a) b)

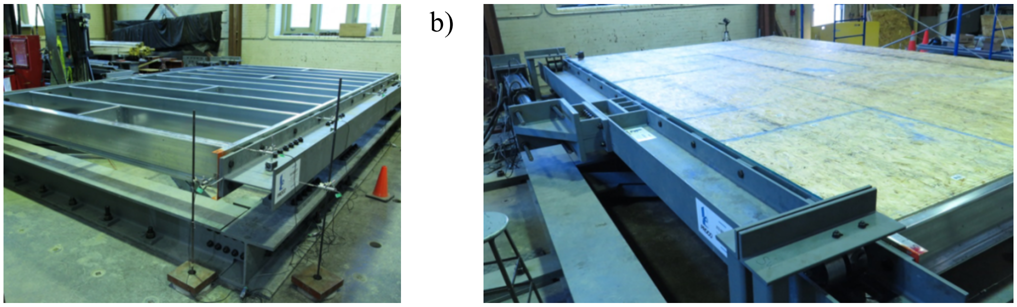

Fig.4. Photographs of diaphragm test specimens; a) unblocked framing prior to installation of OSB sheathing, and b) completed diaphragm with roof sheathing

a)

b)

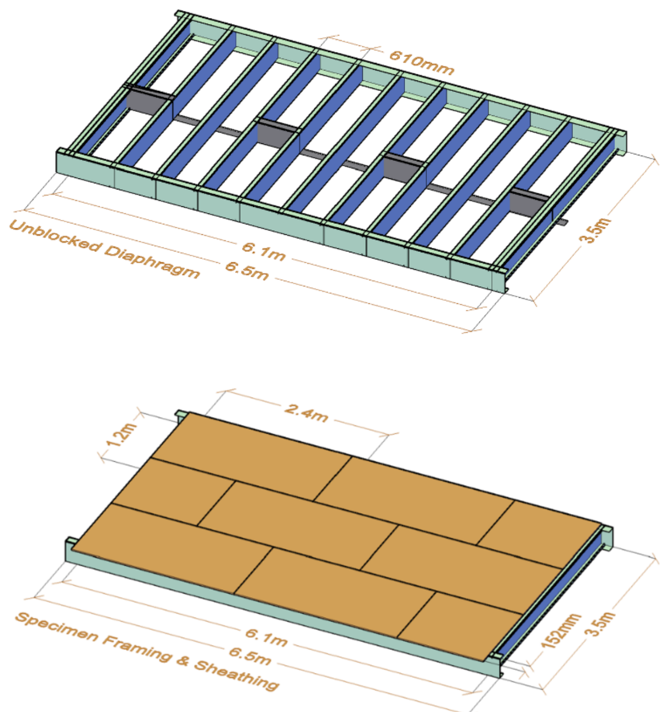

Fig. 5. Illustration of a) CFS framing, and b) wood panel sheathing

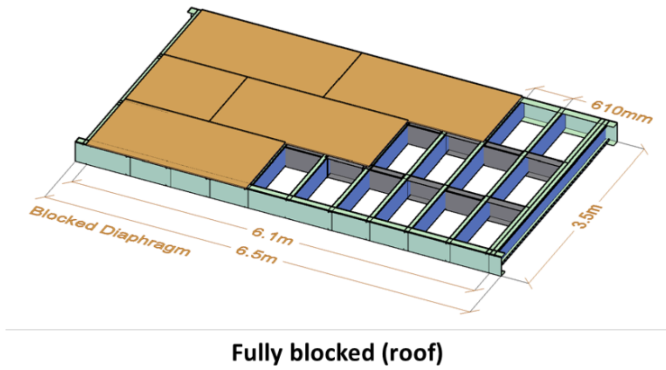

Fig. 6. Modification to the roof diaphragm configurations; full CFS frame blocking

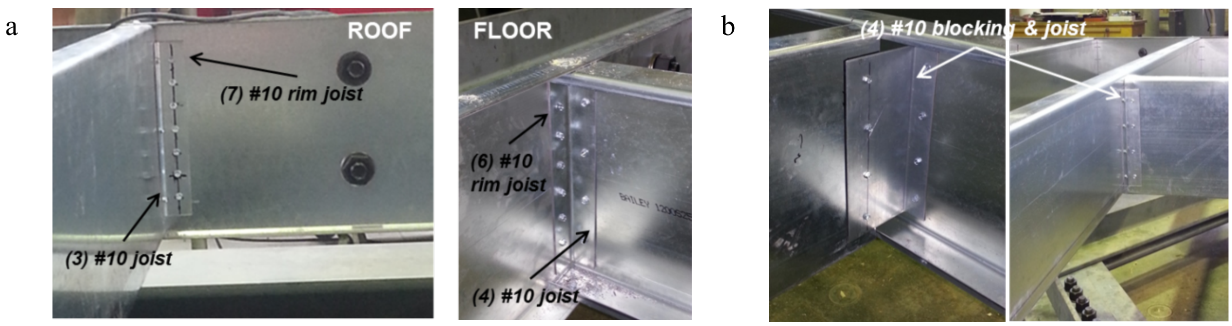

Fig. 7. CFS framing connections; a) joist-to-track connections, and b) blocking-to-joist connections

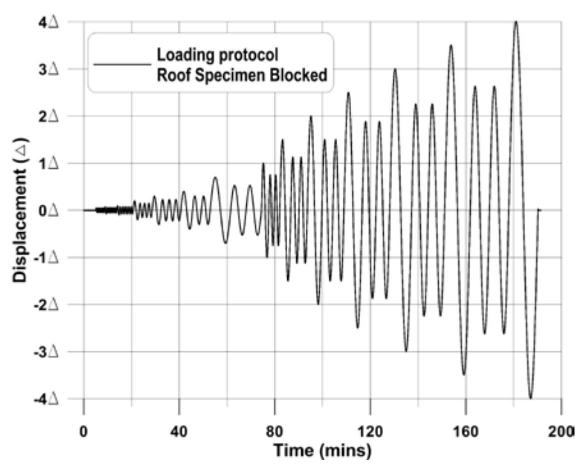

Fig. 8. Consortium of Universities for Research in Earthquake Engineering (CUREE) loading protocol for Specimen 8-RB-C (blocked)

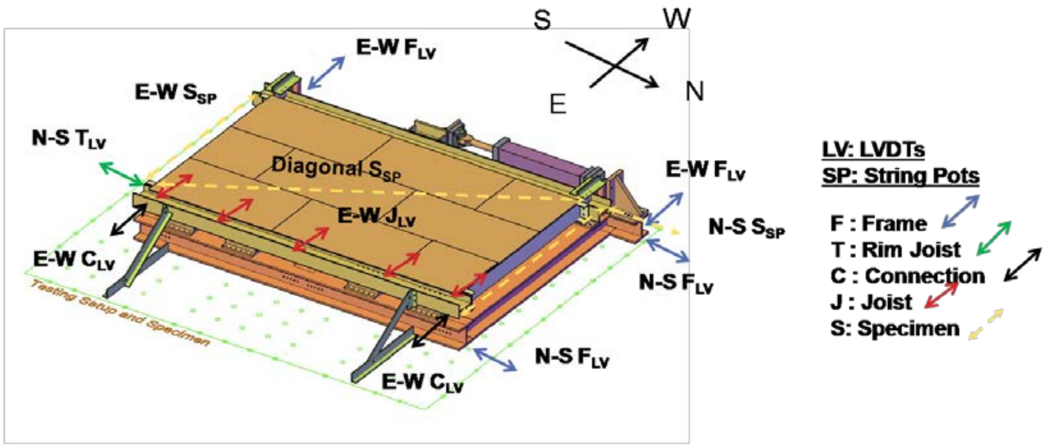

Fig. 9. Instrumentation of diaphragm test specimens

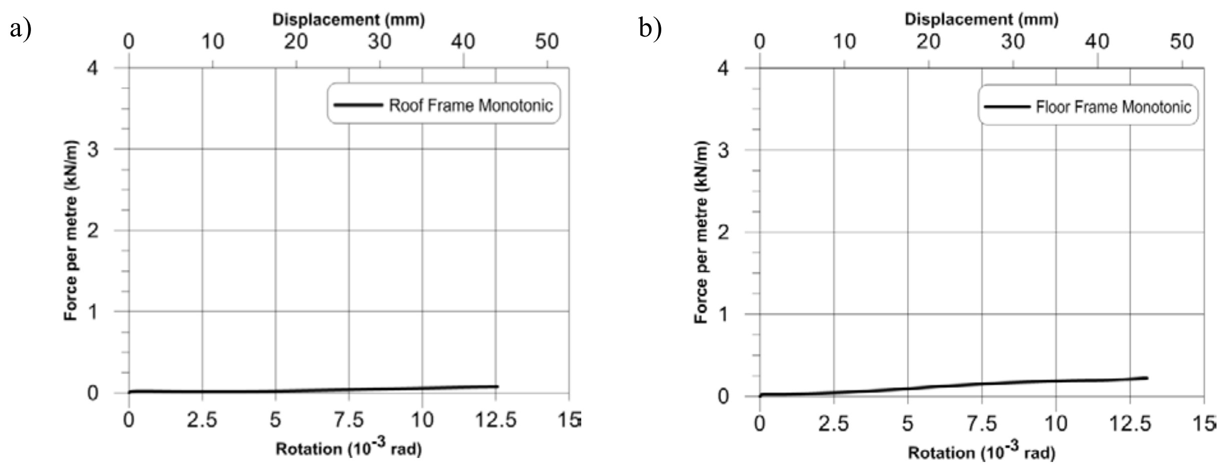

Fig. 10. Shear force vs. rotation response for the bare CFS frame; a) 1-RF-M, and b) 2-FF-M

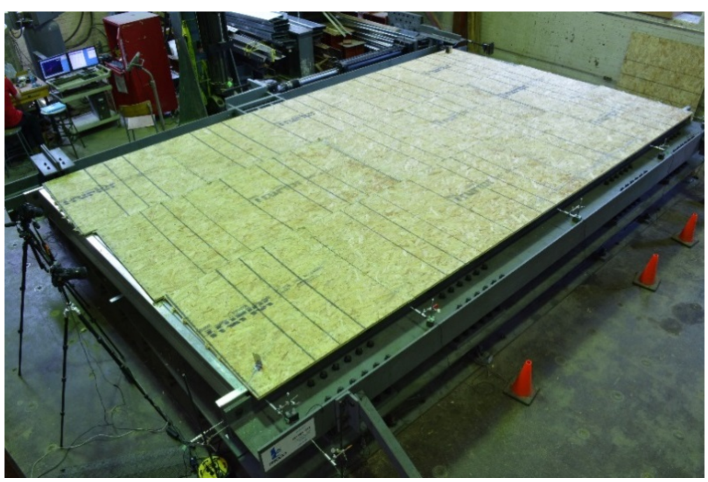

Fig. 11. Example overall shear deformations of typical diaphragm test specimen

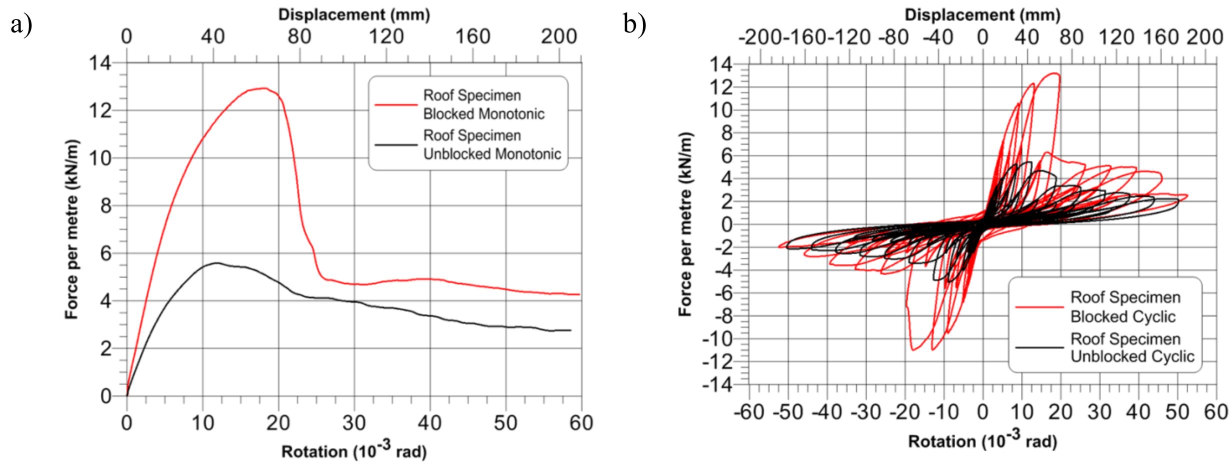

Fig. 12. Force vs. deformation response for roof specimens; a) 3-RU-M (unblocked) &7-RB-M (blocked), and b) 4-RU-C (unblocked) & 7-RB-C (blocked)

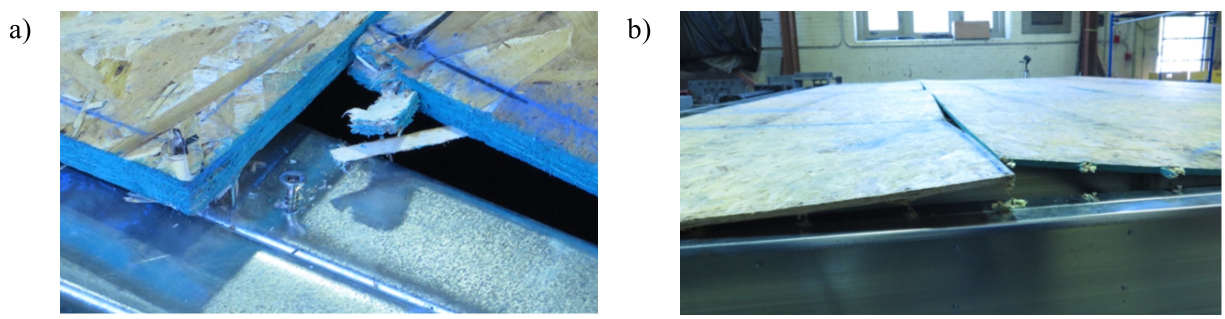

Fig. 13. Deformation for the roof unblocked diaphragm configurations, 3-RU-M & 4-RU-C; a) screw edge tear out, and b) lift-off of OSB panels

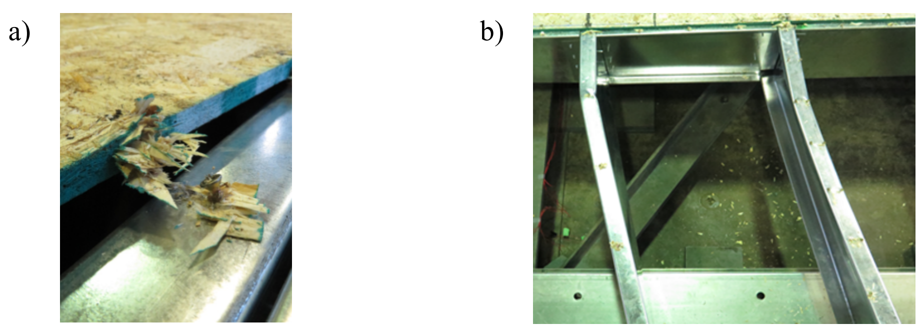

Fig. 14. Deformation for blocked roof diaphragm configuration specimen, 7-RB-M & 8-RB-C; a) screw edge tear out, and b) post-ultimate bending action of steel framing (OSB panels removed for post-test photograph)

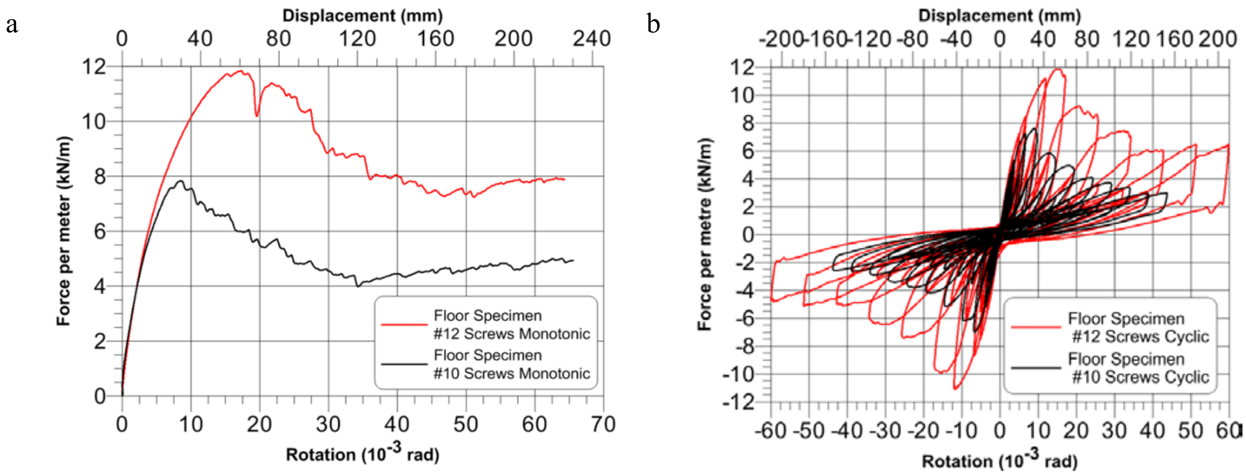

Fig. 15. Force vs. deformation response for floor specimens; a) 5-F#10-M & 9-F#12-M, and b) 6-F#10-C & 10-F#12-C

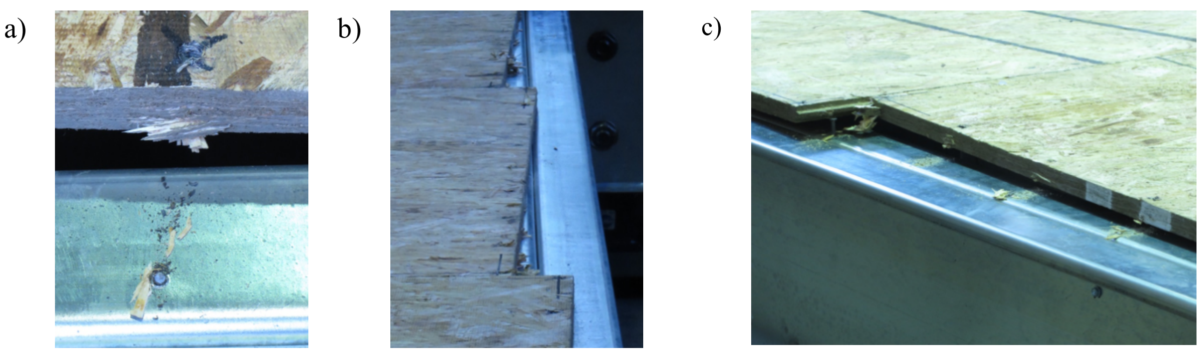

Fig. 16. Deformation for floor diaphragm configurations with #10 screws, 5-F#10-M & 6-F#10-C; a) screw edge shear failure, b) relative displacement between panels, and c) panel edge contact effect